

Simulating urban heat islands and local winds in the Dhaka metropolitan area, Bangladesh

Abeda Tabassum, Seong-Ho Hong, Kyeongjoo Park, Jong-Jin Baik*

School of Earth and Environmental Sciences, Seoul National University, Seoul 08826, South Korea



ARTICLE INFO

Keywords:

Urban heat island
Surface roughness
Local winds
Urban breeze circulation
Dhaka
WRF model

ABSTRACT

Weather and climate changes due to urbanization are of great concern. This study examines urban effects on thermal and wind environments in the Dhaka metropolitan area, Bangladesh. For this, simulations for a case of hot days with weak synoptic forcing are performed using the Weather Research and Forecasting (WRF) model. The differences between the urban and no-urban simulations are analyzed. In the urban simulation, the daytime sensible (latent) heat flux is considerably increased (reduced) and convective activities are enhanced. The nighttime (0000–0500 LST) urban heat island (UHI) is much stronger than the daytime (1200–1700 LST) UHI. In the daytime, the UHI effect on local winds is more important than the urban surface roughness effect. In the nighttime, the relative importance of the UHI and urban surface roughness effects differs depending on the region for given prevailing winds. Impacts of increases in anthropogenic heat and urban size are examined. As the anthropogenic heat increases, the UHI and the UHI effect on local winds strengthen. As the urban size increases, the UHI and the UHI effect on local winds strengthen and the surface roughness effect appears in wider areas. This study provides further insights into urban effects on local winds.

1. Introduction

Urbanization is accompanied by the replacement of natural surfaces with impervious surfaces which are mainly comprised of man-made materials such as asphalt and concrete (Weng, 2012). In the daytime, impervious surfaces tend to more absorb incoming shortwave radiation and thus more store heat into the subsurface than natural surfaces (Phelan et al., 2015). Furthermore, compared to natural surfaces, impervious surfaces cause less evapotranspiration and more sensible heat transfer from the surface to near-surface air (Kuang et al., 2015). In the nighttime, the release of stored heat to the near-surface air is more prominent at impervious surfaces than at natural surfaces (Ramamurthy et al., 2014). These distinct characteristics of impervious surfaces contribute to urban areas being warmer than their surrounding rural areas which is called the urban heat island (UHI) (Memon et al., 2008). The UHI is evident in numerous cities around the world and is typically stronger in the nighttime than in the daytime near the surface (Du et al., 2021). In warm seasons, the UHI is responsible for increases in the occurrences of heat waves and tropical nights in urban areas, implying its significant roles in aggravating urban thermal environment (Tan et al., 2010; Choi and Lee, 2019).

Urbanization influences local winds through the UHI and the enhancement of surface roughness (Rajeswari et al., 2022; Zheng et al., 2024). The UHI produces pressure differences between urban areas and their surrounding rural areas, thereby inducing a mesoscale circulation called the urban breeze circulation (UBC) (Hong et al., 2024). The UBC is characterized by converging flows

* Corresponding author.

E-mail address: jjbaik@snu.ac.kr (J.-J. Baik).

toward urban areas in the lower atmosphere and diverging flows toward their surrounding rural areas above it (Lemonsu and Masson, 2002; Wang and Li, 2016). The UBC interacts with prevailing winds (Zhang et al., 2014; Wang et al., 2020a) and also with updrafts and downdrafts that are formed in the convective boundary layer (Ryu et al., 2013a; Hong et al., 2024), modifying local winds in and around urban areas. Meanwhile, the enhanced surface roughness due to urban built structures decelerates or diverts prevailing winds in and around urban areas (Cotton and Pielke, 2007; Wever, 2012; Zhang et al., 2019). These two urban effects on local winds have been reported to be important in characterizing wind environments in and around many cities (Kang et al., 2014; Yang et al., 2020; Brandi et al., 2024).

Dhaka, the capital of Bangladesh, is one of the megacities in Asia, with a population of 10.3 million and a population density of 33,650 km⁻² (BBS, 2022). The climate of Dhaka belongs to a tropical savannah climate (Aw) in the Köppen-Geiger classification (Beck et al., 2018). The annually averaged temperature is ~26 °C in Dhaka (Tabassum et al., 2024). In the pre-monsoon season (March to May) which is the hottest season, heat waves often occur in Bangladesh (Nissan et al., 2017) and the mean daily maximum temperature in Dhaka is ~34 °C (Uddin et al., 2022). Dhaka has undergone rapid urbanization during the past decades (Byomkesh et al., 2012). This has led to the exacerbation of heat-related risks in this city (Imran et al., 2021). Since Dhaka and its nearby areas are projected to be further urbanized (UN DESA, 2019; Kotharkar and Ghosh, 2021), understanding urban effects on local weather and climate in these regions is greatly important for mitigating or preventing weather- and climate-related risks.

Urban effects on temperature in Dhaka have been studied through observational analysis and numerical simulation (Ahmed et al., 2013; Das and Karmakar, 2015; Imran et al., 2021; Abrar et al., 2022; Uddin et al., 2022; Tabassum et al., 2024). Imran et al. (2021) analyzed satellite-derived land surface temperatures and showed that the annually averaged land surface temperature in Dhaka increases by 0.24 °C per year during 1993–2020 due to urbanization. Using near-surface observations, Tabassum et al. (2024) reported that the annually averaged UHI intensity in Dhaka increases by 0.21 °C per decade during 1995–2019. Das and Karmakar (2015)

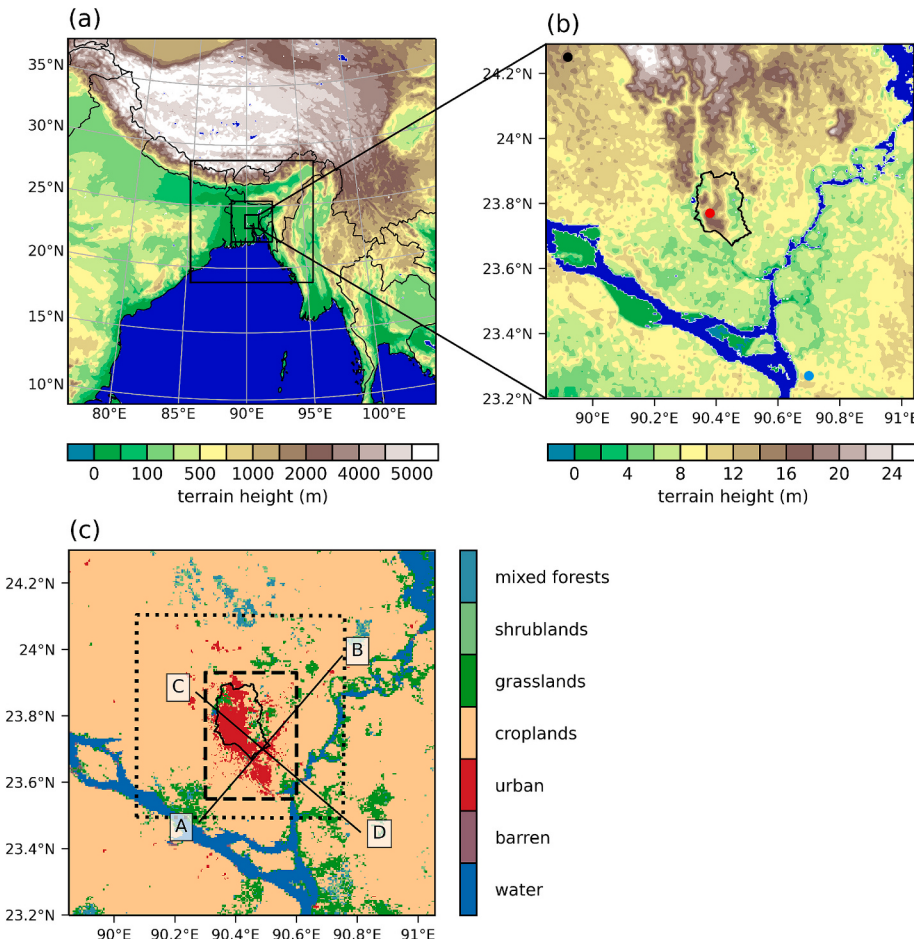


Fig. 1. (a) Four domains with terrain height (shaded), (b) innermost domain with terrain height (shaded), and (c) innermost domain with land cover. The locations of Dhaka (red dot), Chandpur (blue dot), and Tangail (black dot) meteorological stations are marked in (b). The administrative boundary of Dhaka is indicated by the black line in (b) and (c). The analysis area is indicated by the black dotted rectangle in (c). The area within which the urban grids are replaced with cropland in the NO-URBAN simulation is indicated by the black dashed rectangle in (c). (For interpretation of the references to colour in this figure legend, the reader is referred to the web version of this article.)

showed that the simulated UHI intensity in Dhaka reaches up to 7.5 °C for a case in the pre-monsoon season.

Although previous studies have investigated the UHI in Dhaka, several important aspects of the UHI such as its horizontal and vertical structures are yet to be examined in detail. Furthermore, urban effects on local winds in Dhaka have not been studied, although these are important for understanding thermal and wind environments in urban areas. Thus, this study aims to understand urban effects on temperature and local winds in and around Dhaka through high-resolution simulations. For this, a case of hot days is selected. Given that Dhaka is characterized by flat terrain and distant from seas, urban effects on local winds are expected to be discernable in Dhaka and its nearby areas. This enables a detailed examination of urban effects on local winds, which may lead to a better understanding of the urban effects. Furthermore, in view of the rapid urbanization in and around Dhaka, we examine how the urban effects in these regions change with increasing anthropogenic heat and urban size. This examination can give insights into changes in the different effects of the UHI and urban surface roughness on local winds with further urbanization.

2. Numerical model, simulation setup, and analysis method

The numerical model used to simulate urban heat islands and local winds in the Dhaka metropolitan area is the Weather Research and Forecasting (WRF) model version 4.1.3 (Skamarock et al., 2019). The selected physical parameterization schemes are the Dudhia shortwave radiation scheme (Dudhia, 1989), the Rapid Radiative Transfer Model (RRTM) longwave radiation scheme (Mlawer et al., 1997), the Yonsei University (YSU) planetary boundary layer (PBL) scheme (Hong et al., 2006), the unified Noah land surface model (Tewari et al., 2004), the revised MM5 surface layer scheme (Jiménez et al., 2012), the WRF double moment 6-class microphysics scheme (Lim and Hong, 2010), and the Kain-Fritsch convection scheme (Kain, 2004). The Seoul National University Urban Canopy Model (SNUUCM) (Ryu et al., 2011) is implemented into the WRF model to better simulate physical processes occurring in urban areas. The SNUUCM is a single-layer urban canopy model that parameterizes urban physical processes such as absorption and reflection of radiations, turbulent energy exchanges between surface and air, and conduction of heat through the subsurface (Ryu et al., 2011).

Four computational domains considered in this study are shown in Fig. 1a. The one-way nesting option is used. The horizontal grid sizes are 9, 3, 1, and 0.333 km for the four domains. In the horizontal direction, the number of grid points is 379×379 for all the four domains. Note that only the outermost domain uses the Kain-Fritsch convection scheme. In the vertical direction, total 43 layers are

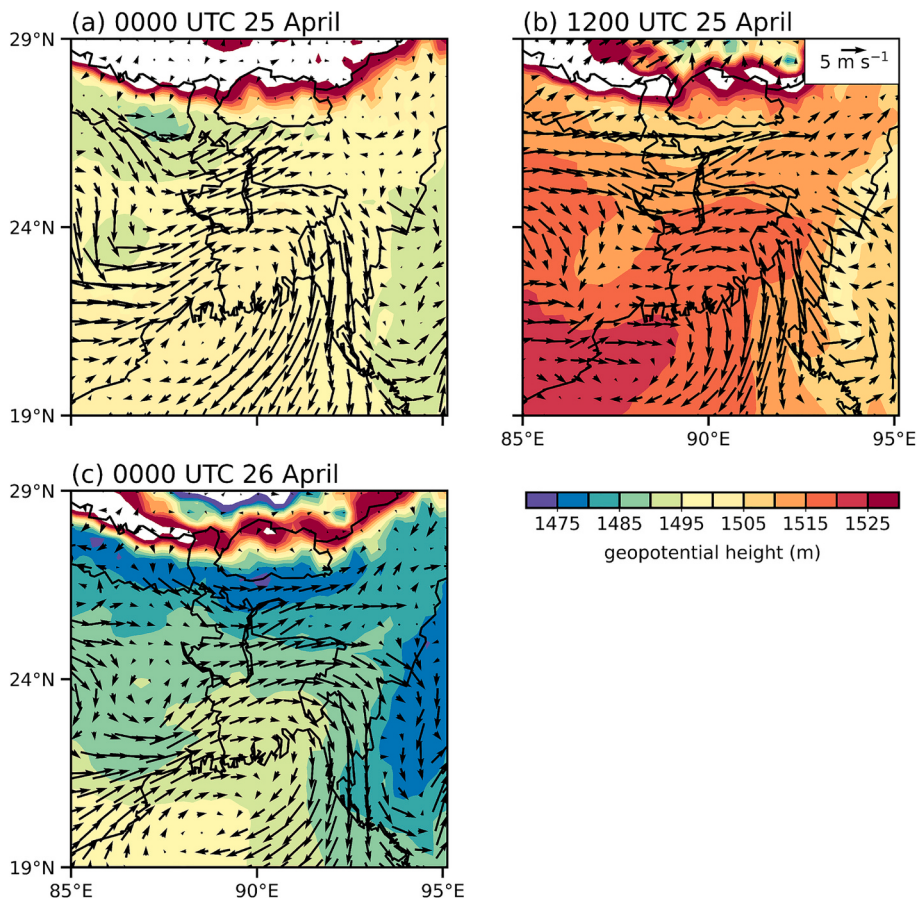


Fig. 2. 850-hPa geopotential height (shaded) and horizontal wind vector fields at (a) 0000 UTC 25, (b) 1200 UTC 25, and (c) 0000 UTC 26 April in 2021.

considered with finer vertical resolutions in the lower atmosphere and the model-top pressure level is 20 hPa. The sixth-order spatial filter is employed to dampen the waves having horizontal wavelengths of 2–4 times the horizontal grid size (Knievel et al., 2007).

Fig. 1b shows the topography in the innermost domain. In this study, the Global Multi-resolution Terrain Elevation Data 2010 (GMTED2010) with a spatial resolution of 30 s (~ 1 km) (Danielson and Gesch, 2011) is used for topography data. Dhaka is located at the center of the deltaic plain of the Ganges, Brahmaputra, and Meghna Rivers, and therefore is characterized by flat terrain, with an average height of 20 m above mean sea level (Montes et al., 2021). The two largest rivers in Bangladesh, the Padma and the Meghna, flow on the west and the east of Dhaka, respectively. For land cover, the Moderate Resolution Imaging Spectroradiometer (MODIS) dataset of 15 s (~ 500 m) resolution (Sulla-Menashe and Friedl, 2018) provided by the National Centers for Environmental Prediction (NCEP) is used. This dataset well represents the land cover in the innermost domain but underestimates the area of the urban land cover in and around Dhaka. For a more precise representation of the land cover, the urban area is updated based on a land cover map created from the Landsat 8 image (Roy et al., 2014). The Landsat 8 provides the image of the global land surface with 30-m resolution in visible, thermal infrared, and shortwave infrared bands (Roy et al., 2014). To generate the land cover map using the Landsat 8 image, the supervised classification technique, which is frequently used for urban land cover mapping and urban change detection (Deng et al., 2009; Raziq et al., 2016), is used. This study utilizes the minimum distance algorithm (Wacker and Landgrebe, 1972) of the supervised classification that requires developing spectral signatures of known categories to allow the software to classify each image pixel into the closest signature. The updated land cover map is presented in Fig. 1c. Note that urban areas exist south of Dhaka as well as inside Dhaka. The simulation conducted with the updated land cover map is called the URBAN simulation. The values of the urban parameters in the SNUUCM follow those of Ryu and Baik (2013). Following Ryu et al. (2013a), a diurnally varying anthropogenic heat profile is considered. In the profile, the daily maximum value is set to 81 W m^{-2} . To investigate the effects of urban land cover in and just around Dhaka, an additional simulation is conducted by replacing the urban grids within the 23.54–23.93°N and 90.26–90.64°E area (black dashed rectangle in Fig. 1c) with cropland and is called the NO-URBAN simulation.

The simulation period is 48 h from 0000 UTC (= 0600 LST) 24 April in 2021. The outermost domain has a time step of 18 s, and each of the inner domains has the time step that is one-third of its parent domain. As the initial and boundary conditions, the fifth-generation European Centre for Medium-range Weather Forecasts (ECMWF) reanalysis (ERA5) data with 1-h temporal resolution and 0.25° spatial resolution (Hersbach et al., 2020) are used. For more realistic simulation, the analysis nudging is applied above the PBL using the ERA5 data. All the analyses are made using the simulation data in the innermost domain. In this study, the periods of 1200–1700 LST and 0000–0500 LST are considered to calculate the daytime and nighttime averages, respectively.

3. Synoptic weather and model validation

During the analysis period, Bangladesh experienced an extreme heat wave with the decade's highest temperature of 41.2 °C (Mannan et al., 2022). Fig. 2 shows the 850-hPa synoptic fields at three different times. At 0000 UTC 25 April, an anticyclonic high-pressure system is dominant over Bangladesh, its center being located at the southwest of Bangladesh. The synoptic wind is very weak over the Dhaka metropolitan area. 12 h later, the anticyclonic flow is still dominant over Bangladesh, with westerly synoptic wind over the Dhaka metropolitan area. At 0000 UTC 26 April, the high-pressure system moves southeastward, the Dhaka metropolitan area being under the northeastern edge of the system. Affected by the high-pressure system, the weather is clear. The 850-hPa wind speed averaged over the 23.25–24.25°N and 90.00–91.00°E area, which includes Dhaka, is 2.5 m s^{-1} at 0000 UTC 25, 3.9 m s^{-1} at 1200 UTC 25, and 4.1 m s^{-1} at 0000 UTC 26 April. These conditions are favorable for the development of local winds.

The 2-m temperature simulated by the WRF model is validated using observation data from three meteorological stations (Dhaka, Chandpur, and Tangail). We used the 3-hourly 2-m temperature observation data obtained from the Bangladesh Meteorological Department. The scatterplot of the simulated 2-m temperature versus the observed 2-m temperature at the three stations during the analysis period is presented in Fig. 3. The WRF model underestimates the 2-m temperature with a mean bias error (MBE) of $-0.60 \text{ }^{\circ}\text{C}$, and the root mean square error (RMSE) is $1.71 \text{ }^{\circ}\text{C}$. The correlation coefficient is 0.95, well capturing the variation of the 2-m

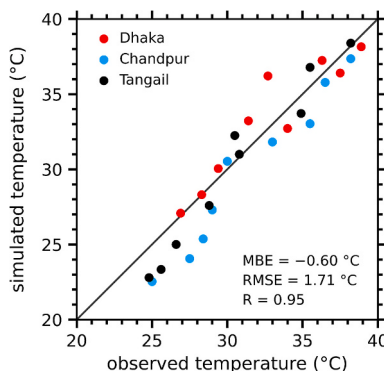


Fig. 3. Scatterplot of simulated versus observed 2-m temperatures at the locations of Dhaka (red), Chandpur (blue), and Tangail (black) meteorological stations. The mean bias error (MBE), root mean square error (RMSE), and correlation coefficient (R) are given. (For interpretation of the references to colour in this figure legend, the reader is referred to the web version of this article.)

temperature. The WRF model overall better simulates the 2-m temperature in the urban area than in the rural area. The MBE (RMSE) is 0.45°C (1.51°C) at the location of Dhaka station, -1.70°C (2.08°C) at the location of Chandpur station, and -0.54°C (1.46°C) at the location of Tangail station, which indicates the capability of the SNUUCM to well simulate near-surface air temperature in the urban area. Overall, the simulation data from the WRF model employed in this study appear to be appropriate to investigate UHIs and local winds in the Dhaka metropolitan area.

4. Results and discussion

4.1. Near-surface and surface temperatures and surface energy fluxes

First, the diurnal variations of near-surface and surface temperatures in the URBAN and NO-URBAN simulations are examined in Fig. 4. After sunrise, the 2-m temperature begins to increase in both simulations (Fig. 4a). From 0840 to 1210 LST, the temperatures in both simulations are nearly identical, with the temperature being marginally higher in the URBAN simulation. In the URBAN simulation, the temperature reaches a peak of 38.0°C at 1540 LST. The peak temperature in the NO-URBAN simulation (37.6°C) occurs 40 min earlier. Both simulations show a decrease in afternoon temperatures; however, the rate of decrease is higher in the NO-URBAN simulation due to faster radiative cooling of rural surface (Chow and Roth, 2006; Lee and Baik, 2010). The 2-m temperatures in both simulations decrease at a similar rate from sunset to sunrise. The 2-m temperature in the URBAN simulation is higher than that in the NO-URBAN simulation in both daytime and nighttime, indicating the presence of the UHI throughout the day. The UHI intensity clearly decreases from 2.69 to 0.39°C during 0600–0740 LST and does not significantly change during 0740–1600 LST. During 1600–1810 LST, the UHI intensity increases from 0.54 to 2.97°C . After sunset, the UHI intensity remains strong with relatively less change than those near sunrise and sunset. This diurnal pattern of the UHI intensity agrees with those observed in many cities (e.g., Wouters et al., 2013; Xue et al., 2023). The daytime- and nighttime-averaged UHI intensities are 0.43 and 3.17°C , respectively, the UHI being pronounced in the nighttime.

In both URBAN and NO-URBAN simulations, the surface temperature exhibits a larger diurnal variation than the 2-m temperature (Fig. 4b). The diurnal range in the URBAN (NO-URBAN) simulation is 26.5 – 38.0°C (23.8 – 37.6°C) for 2-m temperature and 28.4 – 53.3°C (23.0 – 48.8°C) for surface temperature. During 0730–0930 LST, the difference between the surface temperatures in the two simulations is very small ($< 1.5^{\circ}\text{C}$). At noon, the surface temperature is much higher in the URBAN simulation than in the NO-URBAN simulation. In the URBAN simulation, the peak surface temperature is 53.3°C at 1300 LST, occurring 30 min later than that in the NO-URBAN simulation. The surface temperatures in both simulations decrease rapidly during 1320–1820 LST, and their decreasing rates are reduced after sunset. Similar to the UHI intensity, the surface UHI intensity decreases from 5.40 to 1.00°C during 0600–0740 LST. On the other hand, the surface UHI intensity increases from 1.07 to 8.73°C during 0910–1800 LST, dissimilar to the UHI intensity. The overall increase in surface UHI intensity in the daytime is also found in some previous studies (Zhou et al., 2013; Sismanidis et al., 2015). After sunset, the surface UHI intensity exhibits a relatively slight variation from 5.53 to 8.61°C . The daytime- and nighttime-averaged surface UHI intensities are 5.83 and 6.26°C , respectively, the surface UHI being higher in the nighttime than in the daytime.

Next, the diurnal variations of surface energy fluxes are examined. Fig. 5 shows the incoming/outgoing shortwave and longwave radiations in the URBAN and NO-URBAN simulations. The difference in incoming shortwave radiation between the two simulations is

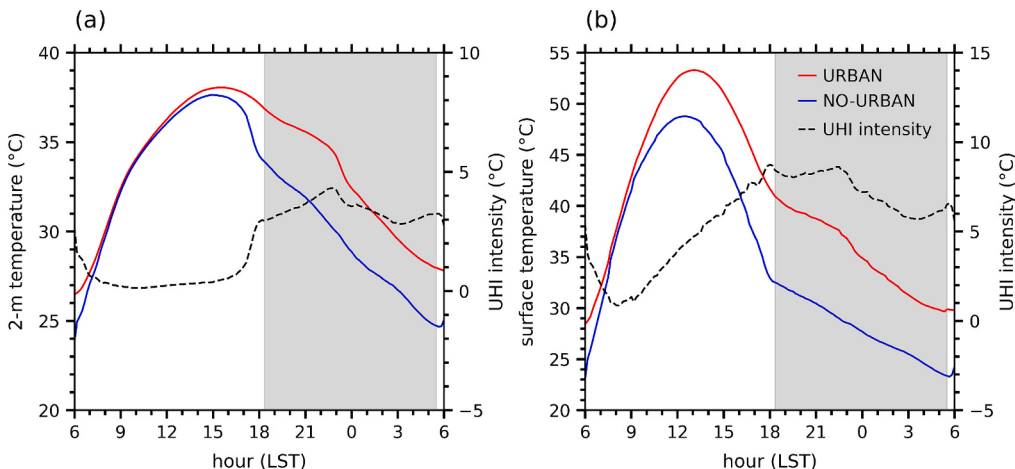


Fig. 4. Diurnal variations of (a) 2-m temperature and (b) surface temperature in the URBAN (red line) and NO-URBAN (blue line) simulations. The variables are averaged over the urban grids within the analysis area in the URBAN simulation and over the corresponding grids in the NO-URBAN simulation. The dashed lines in (a) and (b) indicate the UHI intensity and the surface UHI intensity, respectively. The shaded area indicates the period from sunset to sunrise. (For interpretation of the references to colour in this figure legend, the reader is referred to the web version of this article.)

negligible throughout the analysis period ($< 1 \text{ W m}^{-2}$ in magnitude) (Fig. 5a). The maximum incoming shortwave radiation in the URBAN simulation is 1033 W m^{-2} which is larger than that reported in other mid-latitude cities such as Boston, U.S.A. (Wang and Li, 2021) and Seoul, South Korea (Yi et al., 2022) during heat waves. This is likely attributed, to some or large extent, to that Dhaka is located in a relatively low-latitude region compared to these cities. Meanwhile, the outgoing shortwave radiation is clearly reduced in the URBAN simulation than that in the NO-URBAN simulation (Fig. 5b). This means that the urban surface less reflects incoming shortwave radiation than the rural surface. Sugawara and Takamura (2014) demonstrated that the multiple reflections of shortwave radiation occurring in urban canopies reduce the amount of outgoing shortwave radiation from the urban surface. The outgoing shortwave radiation averaged from sunrise to sunset in the URBAN simulation is 67 W m^{-2} , being 55 % of that in the NO-URBAN simulation. The absorption of shortwave radiation in the URBAN simulation is, therefore, increased than that in the NO-URBAN simulation.

The incoming longwave radiation in the URBAN simulation is consistently increased throughout the analysis period compared to that in the NO-URBAN simulation (Fig. 5c). This is to some extent associated with the fact that the downward longwave radiation strongly depends on air temperature (Oke and Fugle, 1972). The averaged differences in incoming longwave radiation between the two simulations are 12 and 18 W m^{-2} in the daytime and nighttime, respectively. The outgoing longwave radiation in the URBAN simulation is increased by $22\text{--}73 \text{ W m}^{-2}$ during the analysis period compared to that in the NO-URBAN simulation (Fig. 5d). These increases in outgoing longwave radiation are closely associated with the increases in surface temperature due to urban effects (Fig. 4b). The averaged differences in outgoing longwave radiation between the two simulations are 60 and 52 W m^{-2} in the daytime and nighttime, respectively.

The urban effects on turbulent and storage heat fluxes are evident (Fig. 6a–c). Compared to the NO-URBAN simulation, the daytime-averaged sensible heat flux is increased by 182 W m^{-2} in the URBAN simulation (Fig. 6a). The maximum sensible heat flux is 414 W m^{-2} at 1320 LST in the URBAN simulation and 244 W m^{-2} at 1200 LST in the NO-URBAN simulation. The daytime-averaged latent heat flux is reduced by 122 W m^{-2} in the URBAN simulation (Fig. 6b). Compared to the NO-URBAN simulation, the storage heat flux from the surface to the subsurface in the URBAN simulation is increased during 0630–1220 LST, and the storage heat flux from the subsurface to the surface in the URBAN simulation is increased during 1600–0600 LST (Fig. 6c). The averaged difference in storage

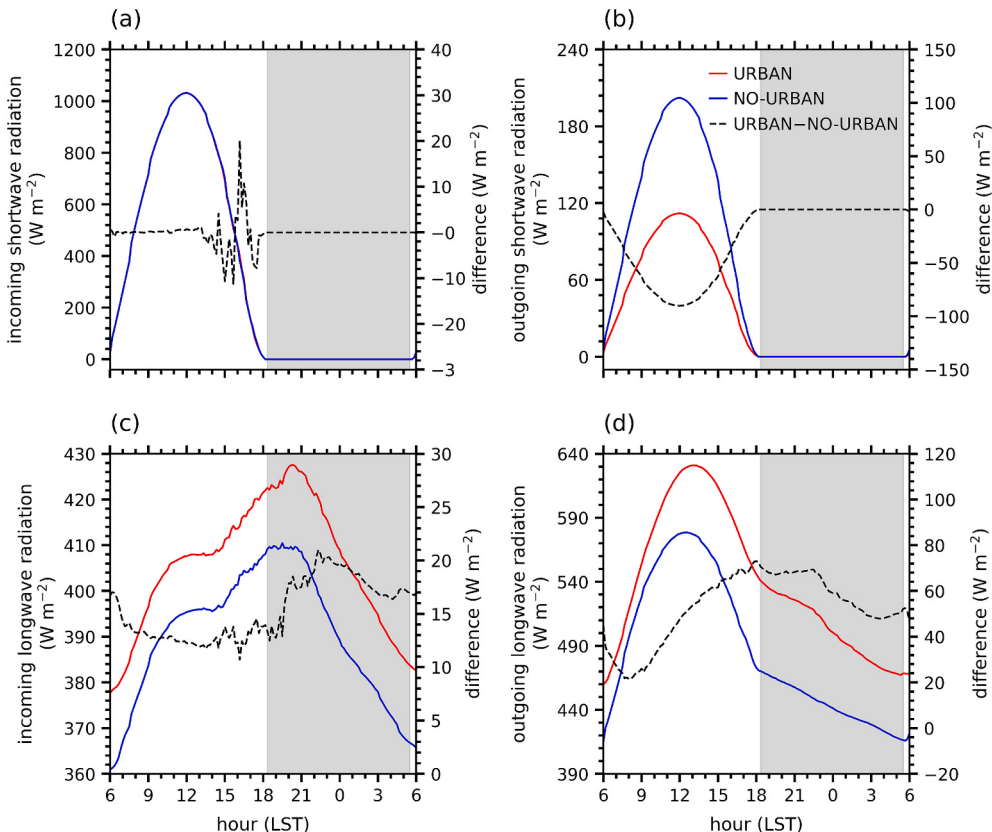


Fig. 5. Diurnal variations of (a) incoming shortwave radiation, (b) outgoing shortwave radiation, (c) incoming longwave radiation, and (d) outgoing longwave radiation in the URBAN (red line) and NO-URBAN (blue line) simulations. The variables are averaged over the urban grids within the analysis area in the URBAN simulation and over the corresponding grids in the NO-URBAN simulation. The black dashed line indicates the difference between the URBAN and NO-URBAN simulations (URBAN minus NO-URBAN). The shaded area indicates the period from sunset to sunrise. (For interpretation of the references to colour in this figure legend, the reader is referred to the web version of this article.)

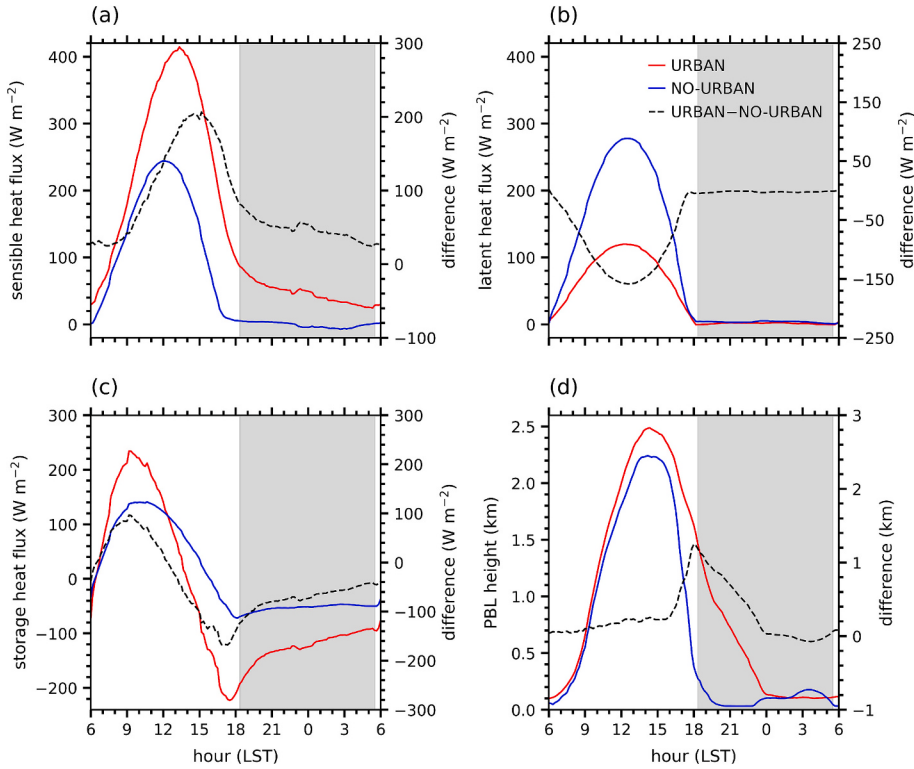


Fig. 6. Diurnal variations of (a) sensible heat flux, (b) latent heat flux, (c) storage heat flux, and (d) PBL height in the URBAN (red line) and NO-URBAN (blue line) simulations. The variables are averaged over the urban grids within the analysis area in the URBAN simulation and over the corresponding grids in the NO-URBAN simulation. The black dashed line indicates the difference between the URBAN and NO-URBAN simulations (URBAN minus NO-URBAN). The shaded area indicates the period from sunset to sunrise. (For interpretation of the references to colour in this figure legend, the reader is referred to the web version of this article.)

heat flux between the two simulations is 56 W m^{-2} during 0630–1220 LST and 59 W m^{-2} during 1600–0600 LST. Both increases in daytime Bowen ratio and the amount of nighttime heat storage are well-known consequences of urbanization (Coutts et al., 2007; Fernández et al., 2021). The PBL height is generally higher in the URBAN simulation than in the NO-URBAN simulation throughout the analysis period (Fig. 6d). This is mainly attributed to the larger sensible heat flux in the URBAN simulation than in the NO-URBAN simulation (Fig. 6a). The maximum PBL height is 2490 m (2243 m) at 1410 LST (1420 LST) in the URBAN (NO-URBAN) simulation. The maximum PBL height in the URBAN simulation is higher or comparable to the maximum PBL heights in other large cities including New York City, U.S.A. (Wu et al., 2019) and Seoul (Baik et al., 2022) during heat waves.

4.2. Urban heat islands and local winds

The urban-rural differences in surface characteristics not only generate the UHI but also induce and/or modify local winds in the Dhaka metropolitan area. The fields of daytime-averaged 2-m temperature and 10-m horizontal wind vectors in the URBAN and NO-URBAN simulations and their differences are shown in Fig. 7a–c. In the NO-URBAN simulation (Fig. 7b), the temperature is relatively high southeast of Dhaka and is relatively low over the rivers. Due to the anticyclonic high-pressure system located southwest of Bangladesh (Fig. 2), the wind speed in and around Dhaka is low ($\sim 2.0 \text{ m s}^{-1}$) and the wind direction is southwesterly west of Dhaka and westerly–northwesterly in and east of Dhaka. In the URBAN simulation (Fig. 7a), the temperature in and downwind of the urban areas is increased by $\sim 0.5^\circ\text{C}$, being noticeably higher than the temperature in the surrounding rural areas. Converging winds are found downwind of the urban areas, and the wind is very weak in the downwind region close to the Meghna River.

Urban effects on temperature and local winds in the daytime are clearly seen in the difference fields (Fig. 7c). The UHI is evident in and downwind of the urban areas, the maximum daytime-averaged UHI intensity in the urban areas being 0.87°C near the center of Dhaka. It is notable that the horizontal wind differences are overall converging. These converging wind differences are indicative of the UBC which is driven by the daytime UHI. The magnitude of the wind difference averaged over the urban areas is 0.5 m s^{-1} in the URBAN simulation. The location of strong convergence is slightly displaced from the urban areas to their downwind regions due to the synoptic (prevailing) winds.

The urban effects in the nighttime when the PBL is stably stratified are distinguished from those in the daytime. The same fields presented in Fig. 7a–c except for the nighttime are shown in Fig. 7d–f. In the NO-URBAN simulation (Fig. 7e), the temperature in and around Dhaka is much lower than that in the daytime due to the nocturnal radiative cooling. Associated with the high-pressure system

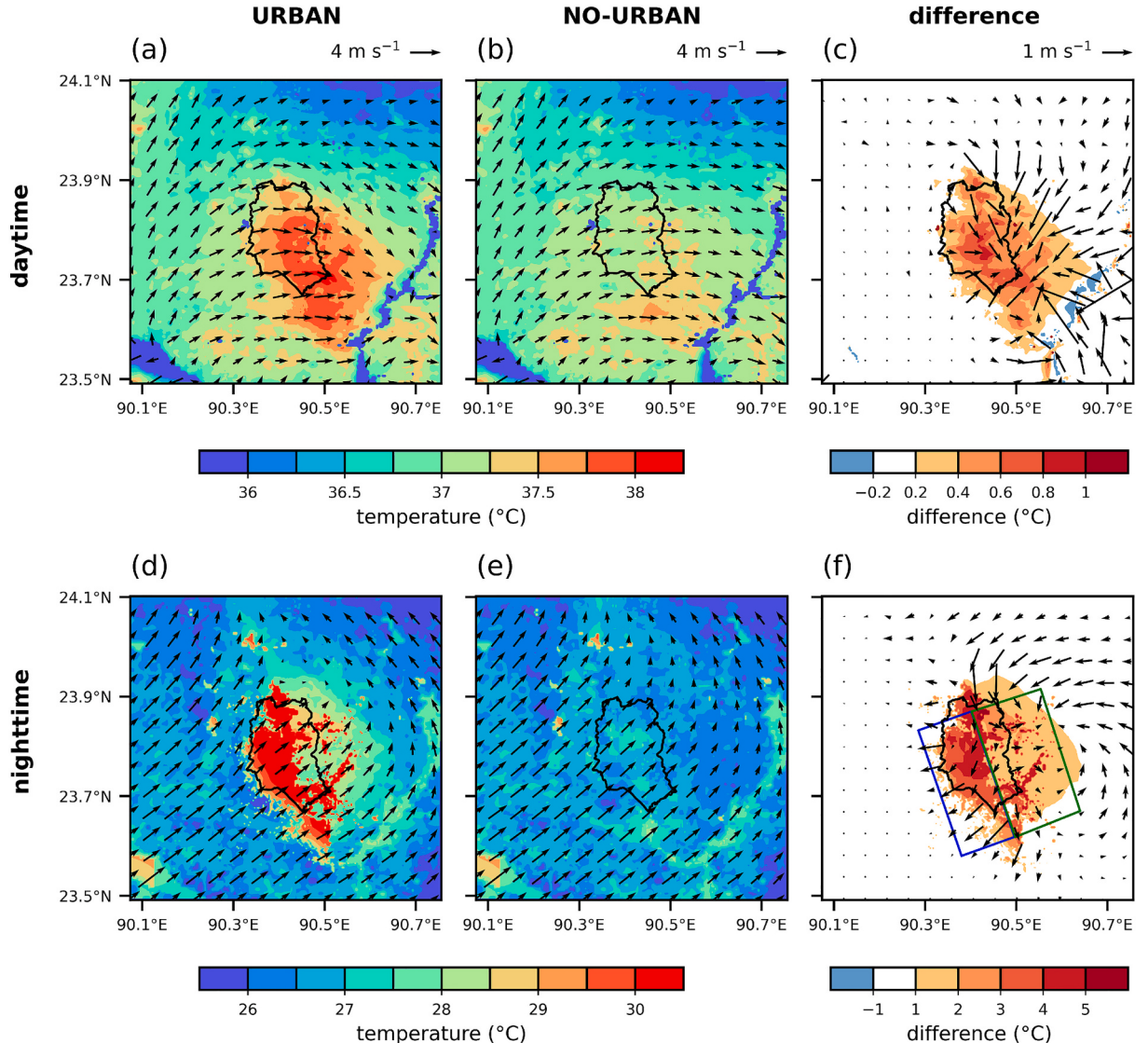


Fig. 7. (a, b) Daytime- and (d, e) nighttime-averaged 2-m temperature (shaded) and 10-m horizontal wind vector fields in the URBAN (first column) and NO-URBAN (second column) simulations and (c, f) their differences (URBAN minus NO-URBAN). The administrative boundary of Dhaka is indicated by the black line. The areas that represent the western region of Dhaka and the eastern region and near-downwind of Dhaka are indicated by the blue and green rectangles in (f), respectively. (For interpretation of the references to colour in this figure legend, the reader is referred to the web version of this article.)

(Fig. 2), the southwesterly wind is prevailing in and southwest of Dhaka (Fig. 7e). The southerly-southeasterly wind is found northeast of Dhaka. In the URBAN simulation, the temperature in the urban areas is significantly increased, exhibiting a strong nighttime UHI (Fig. 7d). The temperature increase downwind of the urban areas is also considerable, although it is less pronounced than that in the urban areas. Compared to the NO-URBAN simulation, in the URBAN simulation, the wind is relatively weak in and around the urban areas.

The difference fields (Fig. 7f) clearly show urban effects on temperature and local winds in the nighttime. A strong nighttime UHI is found in the urban areas. In the downwind of the urban areas, a relatively weak UHI is also seen. The maximum nighttime-averaged UHI intensity is 5.60 °C near the northeastern edge of Dhaka. The difference in horizontal wind vectors reveals interesting features. In the western region of Dhaka, it is seen that the wind differences are overall easterly-northeasterly. The magnitude of the wind difference averaged over the western region of Dhaka (represented by the blue rectangle in Fig. 7f) is 0.6 m s⁻¹. The wind differences along the southwestern border of Dhaka are particularly strong. Enhanced surface roughness in urban areas decelerates prevailing winds (surface roughness effect), while UHIs induce winds blowing toward urban areas (UHI effect). In the western region of Dhaka, the wind differences are directed in approximately opposite direction to southwesterly prevailing winds. This indicates that the surface roughness effect is more important than the UHI effect. Meanwhile, in the eastern region and near-downwind of Dhaka, the wind

differences are relatively weak. The magnitude of the wind difference averaged over the eastern region and near-downwind of Dhaka (represented by the green rectangle in Fig. 7f) is 0.4 m s^{-1} , being smaller than that averaged over the western region of Dhaka. It is also seen that the wind differences are overall converging downwind of Dhaka. These indicate that in the eastern region and near-downwind of Dhaka, the surface roughness effect and UHI effect induce overall opposing wind differences and therefore offset each other, both effects being important.

To examine urban effects on boundary layer structures and the UBC, the vertical cross sections of the daytime-averaged differences in potential temperature and horizontal wind along the line A-B and line C-D between the URBAN and NO-URBAN simulations are presented in Fig. 8. The lines A-B and C-D are selected, since these lines well represent urban effects on boundary layer structures and the UBC (see Fig. 1c). The differences in wind vectors between the two simulations along the lines A-B and C-D are also shown in Fig. 8a and c, respectively. Along the line A-B, potential temperature excesses (i.e., UHI) are extended up to $z \sim 2 \text{ km}$ (Fig. 8a). The maximum daytime-averaged potential temperature excess is found at $x \sim 33 \text{ km}$. In the urban area, potential temperature deficits lie above the potential temperature excesses. The urban breeze converges toward the urban area in the lower PBL and diverges toward the surrounding rural areas in and above the upper PBL, showing a typical structure of the daytime UBC (Fig. 8a and b). The structure of the UBC is asymmetric due to the prevailing winds; the upwind (i.e., left) part of the UBC is contracted and its downwind (i.e., right) part is elongated (Fig. 8b). The maximum intensity of the urban breeze in the lower PBL along the line A-B is 1.6 m s^{-1} . Along the line C-D, potential temperature excesses are found in and downwind (i.e., right) of the urban area (Fig. 8c). The potential temperature excesses are especially large at $x \sim 26 \text{ km}$ and $x \sim 33 \text{ km}$. Over the Meghna River, the PBL height in the URBAN simulation is low. Below $z \sim 1.6 \text{ km}$, the converging urban breeze is apparent (Fig. 8d) and could be influenced by the Meghna River.

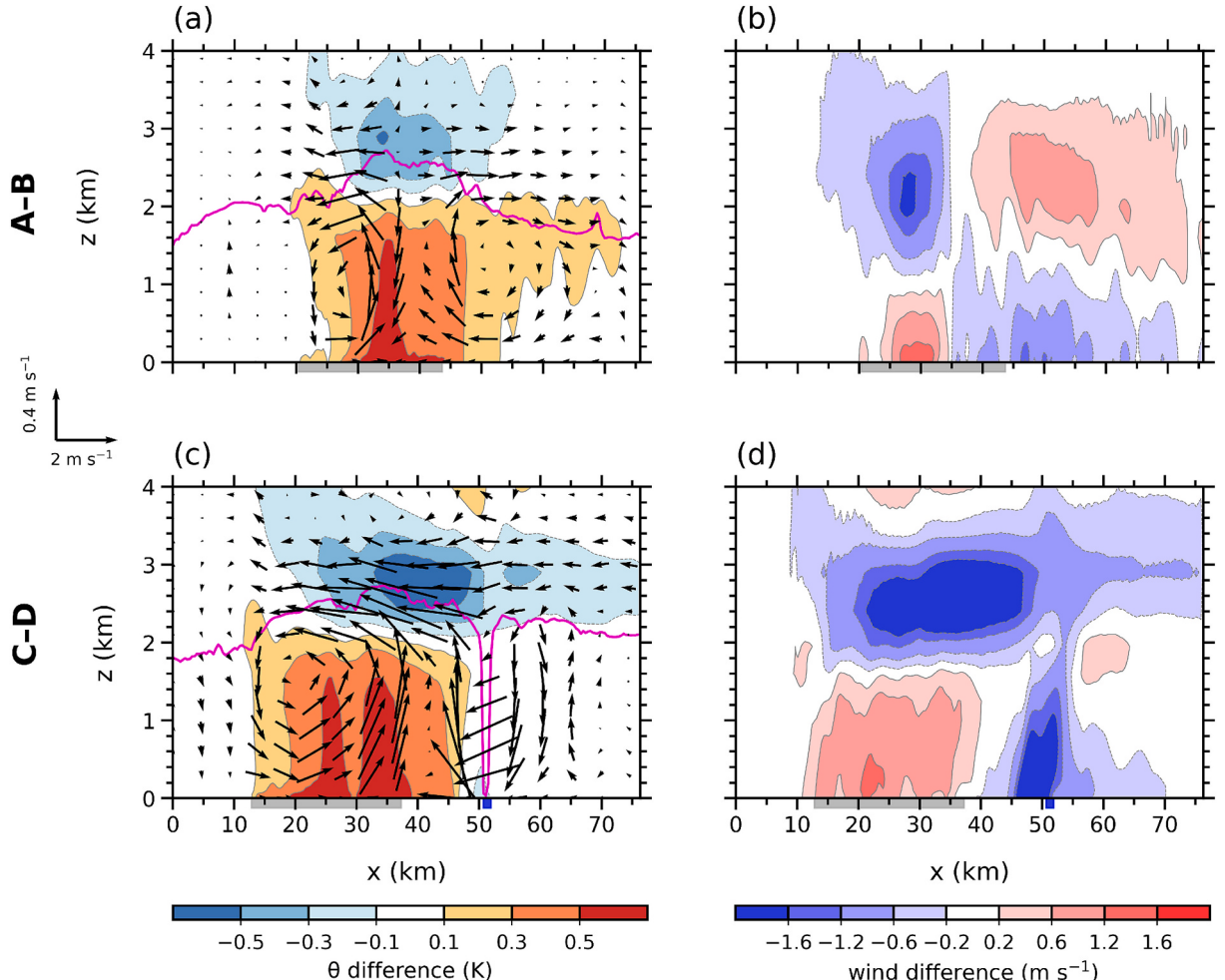


Fig. 8. Vertical cross sections of the daytime-averaged differences in (a, c) potential temperature (shaded) and wind vectors and (b, d) horizontal wind (shaded) along the line A-B (first row) and line C-D (second row) (see Fig. 1c) between the URBAN and NO-URBAN simulations. The daytime-averaged PBL heights in the URBAN simulation are indicated by the pink lines in (a) and (c). The major urban area along each of the lines A-B and C-D is indicated by the grey box on the x-axis. The river is indicated by the blue box on the x-axis in (c) and (d). (For interpretation of the references to colour in this figure legend, the reader is referred to the web version of this article.)

Fig. 9 is the same as **Fig. 8** except for the nighttime-averaged differences in potential temperature and horizontal wind along the line A–B between the two simulations. The difference in wind vectors between the two simulations along the line A–B is also presented in **Fig. 9a**. Strong potential temperature excesses are found within the shallow stable PBL in the urban area. These potential temperature excesses are advected downwind and upward by the prevailing winds (not shown). In the urban area, potential temperature deficits are present above the potential temperature excesses. Pronounced wind differences generally occur over $z \sim 0$ –0.22 km (**Fig. 9b**). In $x \sim 20$ –35 km, a strong negative wind difference is found near the surface, consistent with the deceleration of the prevailing southwesterly winds by the surface roughness effect (**Fig. 7f**). This negative wind difference is advected downwind and upward by the prevailing winds. Meanwhile, the wind difference near the surface is weak in $x \sim 35$ –50 km and is converging in $x \sim 50$ –58 km. These regions are consistent with the eastern region and near-downwind of Dhaka where both surface roughness effect and UHI effect are important.

In summary, for the present simulation case in the Dhaka metropolitan area, in the daytime when the PBL is characterized by the convective boundary layer, the well-developed deep UBC induced by the UHI is formed although the daytime UHI is much weaker than the nighttime UHI. Winds weaken due to larger surface roughness in the urban areas, but the UHI effect plays a crucial role in urban effects on local winds. In the nighttime when the PBL is stable and much shallower than that in the daytime, the relative importance of the UHI and surface roughness effects differs depending on the region for given prevailing winds. In the western region of Dhaka, the surface roughness effect on local winds is more important than the UHI effect on local winds although the nighttime UHI is much stronger than the daytime UHI. In the eastern region and near-downwind of Dhaka, both UHI and surface roughness effects on local winds are important and the UHI effect is largely counteracted by the surface roughness effect. These results for the nighttime are interesting findings of this study.

The UHI and/or surface roughness effects on local winds in inland cities were reported by previous simulation studies. Wang et al. (2020b) investigated local circulations in and around Beijing and Tianjin, China on a day with low-wind speed and clear-sky conditions. They showed that pronounced UBCs are formed in daytime as well as nighttime, which indicates that the UHI effect is important during the whole day. Meanwhile, Brandi et al. (2024) investigated boundary-layer winds in the Phoenix metropolitan area, U.S.A. during a hot and dry summer season. They showed that the surface roughness effect is important during most of the day and that the UHI effect plays minor roles without noticeably changing wind directions. These studies and our results suggest that the relative importance of the UHI and surface roughness effects can considerably differ depending on cities and the synoptic weather conditions. Further investigations in various cities under different weather conditions are needed.

4.3. Daytime convective activities

The daytime convective boundary layer is characterized by updrafts, downdrafts, and their organizations, and these convective activities are influenced by the presence of urban areas. To examine urban effects on convective activities, the fields of horizontal wind vectors and vertical velocity at $z = 500$ m at six different times in the NO-URBAN simulation are analyzed (**Fig. 10**). As the sensible heat flux increases and the PBL develops in the morning (**Fig. 6a** and d), discernible updrafts and downdrafts are formed and develop as shown in **Fig. 10a**. At 1230 LST, the updrafts/downdrafts west of Dhaka exhibit roll-like structures which are elongated in a similar direction to that of the prevailing winds (southwesterly) (**Fig. 10b**). The wavelength and aspect ratio of these structures in the

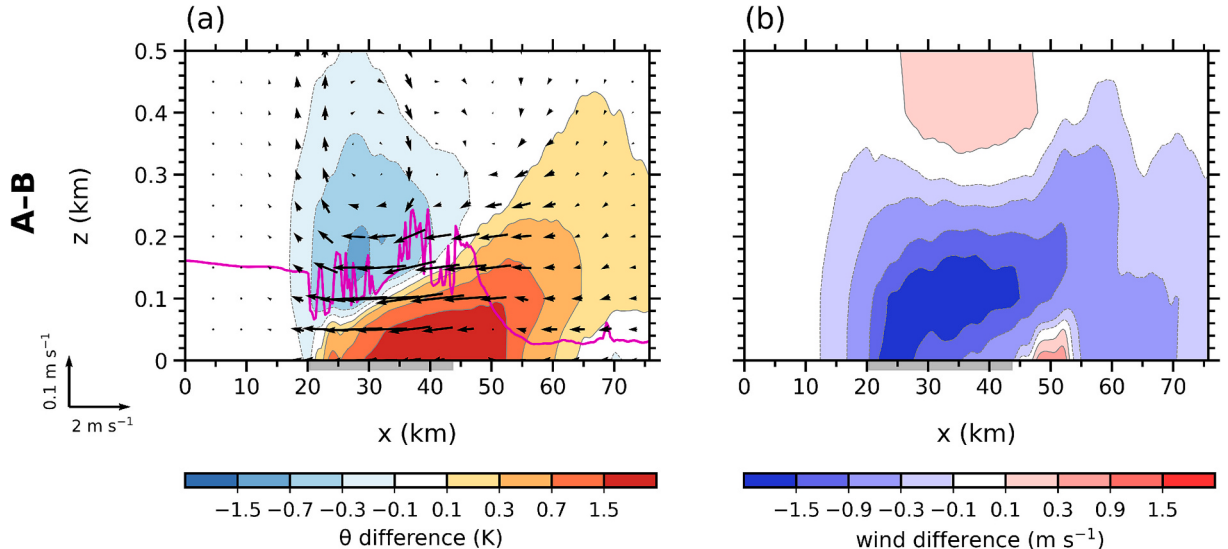


Fig. 9. Vertical cross sections of the nighttime-averaged differences in (a) potential temperature (shaded) and wind vectors and (b) horizontal wind (shaded) along the line A–B (see **Fig. 1c**) between the URBAN and NO-URBAN simulations. The nighttime-averaged PBL height in the URBAN simulation is indicated by the pink line in (a). The major urban area along the line A–B is indicated by the grey box on the x-axis. (For interpretation of the references to colour in this figure legend, the reader is referred to the web version of this article.)

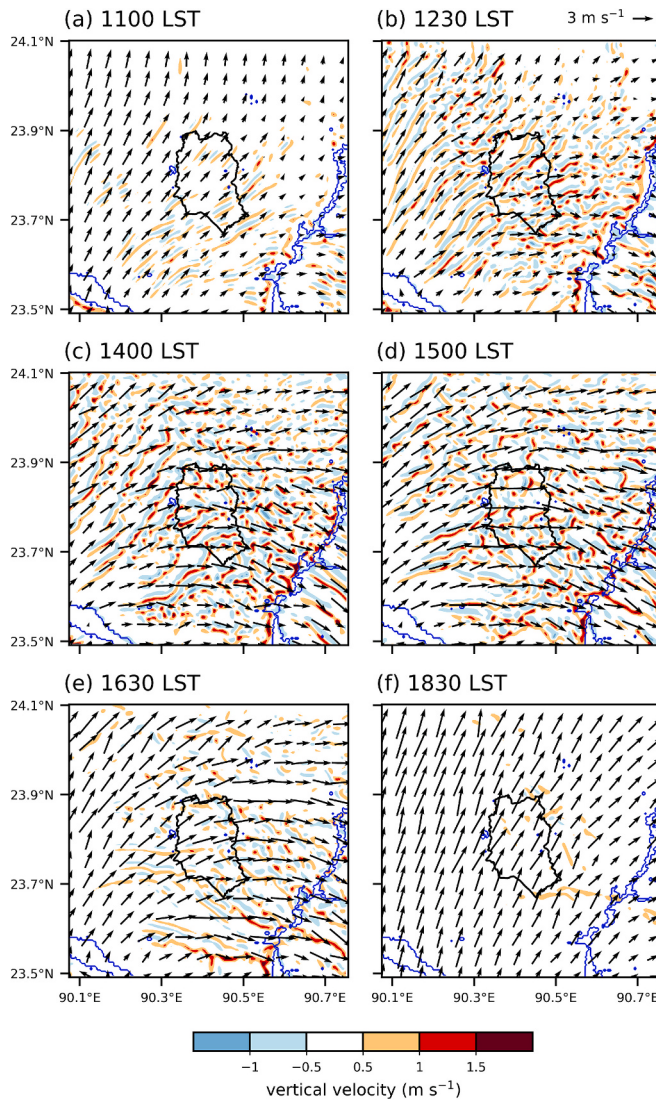


Fig. 10. Horizontal wind vector and vertical velocity (shaded) fields at $z = 500$ m at (a) 1100, (b) 1230, (c) 1400, (d) 1500, (e) 1630, and (d) 1830 LST in the NO-URBAN simulation. The administrative boundary of Dhaka is indicated by the black line. The water bodies are shown in the blue lines. (For interpretation of the references to colour in this figure legend, the reader is referred to the web version of this article.)

$23.70^{\circ}\text{--}23.90^{\circ}\text{N}$ and $90.10^{\circ}\text{--}90.30^{\circ}\text{E}$ area are ~ 3.1 km and ~ 1.8 , respectively. These values are comparable to those found in observational studies (LeMone, 1973; Banghoff et al., 2020). Meanwhile, updrafts/downdrafts are relatively less organized east of Dhaka where winds are weak. At 1400 LST, convective structures are similar to those at 1230 LST but the updrafts/downdrafts are relatively strong (Fig. 10c). Along the western boundary of the Meghna River where convergence occurs under the influence of the river, strong updrafts are found. At 1500 LST, in comparison with 1400 LST, the updrafts/downdrafts overall weaken and convective structures are more disorganized in and around Dhaka (Fig. 10d). The updrafts/downdrafts further weaken at 1630 LST (Fig. 10e). The intensity of updrafts is stronger than the intensity of downdrafts adjacent to the updrafts (Fig. 10a–e). At 1830 LST, the updrafts/downdrafts almost disappear in the NO-URBAN simulation (Fig. 10f).

Daytime convective activities in and around Dhaka show some notable differences when the urban areas are considered (Fig. 11). Updrafts and downdrafts in and around Dhaka in the URBAN simulation develop in the morning and early afternoon, being similar to those in the NO-URBAN simulation (not shown). From mid-afternoon, the differences in convective activities between the URBAN and NO-URBAN simulations begin to be apparent. At 1400 LST, the updrafts in and downwind of Dhaka are stronger in the URBAN simulation (Fig. 11a) than in the NO-URBAN simulation (Fig. 10c). The maximum vertical velocity in the 23.65–23.90°N and 90.30–90.55°E area at 1400 LST is 3.5 m s^{-1} in the URBAN simulation and 2.5 m s^{-1} in the NO-URBAN simulation. The stronger updrafts in the URBAN simulation are associated with the UHI. The updrafts along the western boundary of the Meghna River are stronger in the URBAN simulation than in the NO-URBAN simulation, the maximum vertical velocity being 3.3 m s^{-1} at 1400 LST. The stronger updrafts in and downwind of Dhaka in the URBAN simulation are also evident at 1500 and 1630 LST. It is notable in the

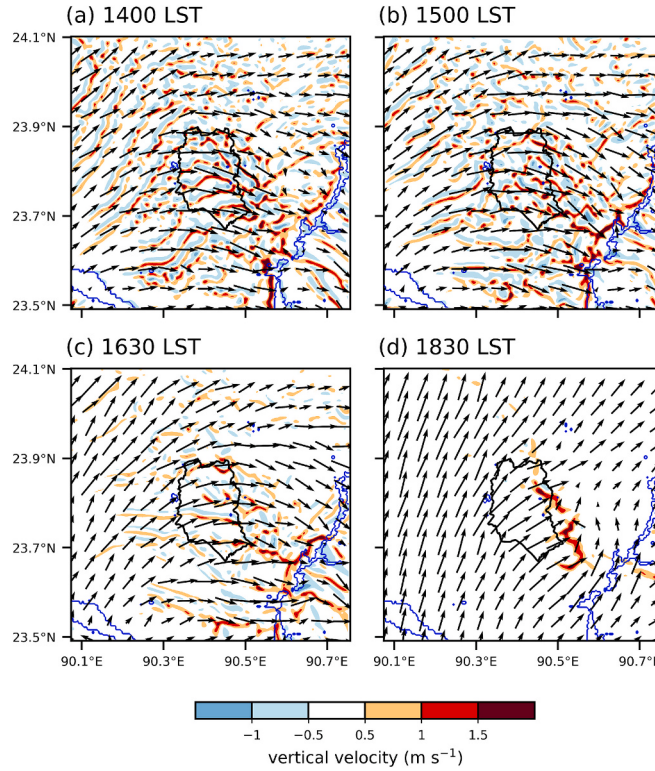


Fig. 11. Same as Fig. 10 except at (a) 1400, (b) 1500, (c) 1630, and (d) 1830 LST for the URBAN simulation.

URBAN simulation that the updrafts along the western boundary of the Meghna River remain strong at 1500 and 1630 LST (Fig. 11b and c), in contrast with the NO-URBAN simulation (Fig. 10d and e). This is likely attributed to the strong convergence associated with urban breeze and the influence of river. At 1830 LST which is right after the sunset (1824 LST), strong updrafts are still evident downwind of the urban areas (Fig. 11d). Figs. 10 and 11 indicate that the UHI acts to invigorate daytime convective activities in and around Dhaka.

4.4. Impacts of increases in anthropogenic heat and urban size

The Dhaka metropolitan area is expected to be further urbanized in the future (UN DESA, 2019; Kotharkar and Ghosh, 2021). In this subsection, how the urban effects on temperature and local winds in the Dhaka metropolitan area change with increasing anthropogenic heat and urban size is examined. To investigate the impact of the increase in anthropogenic heat, two simulations are conducted in which the anthropogenic heat flux is increased to 1.5 times and 2.0 times that in the URBAN simulation. These simulations are called the AH1.5 simulation and AH2.0 simulation, respectively. Simulations with increased urban sizes are also conducted to examine the impact of the increase in urban size. For this, the land cover of the eight grids surrounding each of all urban grids in the $23.54\text{--}23.93^\circ\text{N}$ and $90.26\text{--}90.64^\circ\text{E}$ area, if it is not the urban land cover, is replaced with the urban land cover. When this procedure is applied once and twice, the urban size is increased to 1.7 times and 2.2 times that in the URBAN simulation, respectively. The simulations with these increased urban sizes are called the US1.7 simulation and US2.2 simulation, respectively.

Fig. 12 shows the daytime- and nighttime-averaged differences in 2-m temperature and 10-m horizontal wind vectors between the AH1.5 and NO-URBAN simulations and between the AH2.0 and NO-URBAN simulations. In the daytime, the spatial patterns of the UHI in the AH1.5 and AH2.0 simulations are similar to that in the URBAN simulation but the UHI overall strengthens as the anthropogenic heat increases (Figs. 7c and 12a and b). Compared to the URBAN simulation, the daytime-averaged UHI intensity in the urban areas increases by $0.07\text{ }^\circ\text{C}$ in the AH1.5 simulation and by $0.12\text{ }^\circ\text{C}$ in the AH2.0 simulation. As the UHI strengthens with increasing anthropogenic heat, the converging wind differences are stronger. In comparison with the URBAN simulation, the magnitudes of the wind difference averaged over the urban areas increase by 0.09 and 0.17 m s^{-1} in the AH1.5 and AH2.0 simulations, respectively. Thus, as the anthropogenic heat increases, in the daytime, the UHI is intensified and the UHI effect on local winds is more pronounced. The enhancement of daytime urban breezes with increasing anthropogenic heat is also found in the Seoul metropolitan area (Ryu et al., 2013b).

In the nighttime, the UHI in and around the urban areas overall strengthens with increasing anthropogenic heat (Figs. 7f and 12c and d). In comparison with the URBAN simulation, the nighttime-averaged UHI intensity in the urban areas increases by $0.31\text{ }^\circ\text{C}$ in the AH1.5 simulation and by $0.56\text{ }^\circ\text{C}$ in the AH2.0 simulation. As the UHI intensity increases with increasing anthropogenic heat, the wind

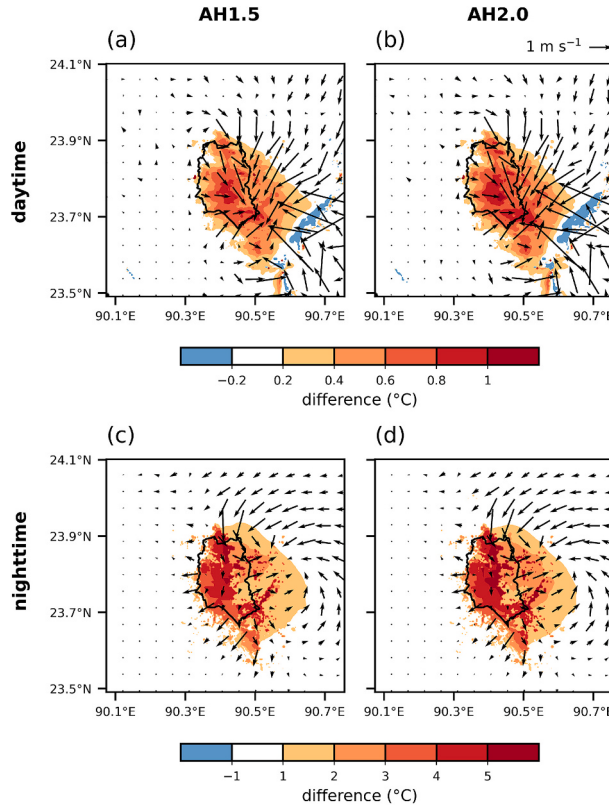


Fig. 12. Fields of the (a, b) daytime- and (c, d) nighttime-averaged differences in 2-m temperature (shaded) and 10-m horizontal wind vectors between the AH1.5 and NO-URBAN simulations (first column) and between the AH2.0 and NO-URBAN simulations (second column). The administrative boundary of Dhaka is indicated by the black line.

differences in the western region of Dhaka are weaker. Compared to the URBAN simulation, the magnitude of the wind difference averaged over the western region of Dhaka (represented by the blue rectangle in Fig. 7f) decreases by 0.09 m s^{-1} in the AH1.5 simulation and by 0.13 m s^{-1} in the AH2.0 simulation. In contrast, the wind differences in the eastern region of Dhaka are stronger as the UHI strengthens with increasing anthropogenic heat. The magnitude of the wind difference averaged over the eastern region and near-downwind of Dhaka (represented by the green rectangle in Fig. 7f) increases by 0.08 m s^{-1} in the AH1.5 simulation and by 0.16 m s^{-1} in the AH2.0 simulation. The changes in the wind difference in and around Dhaka indicate that as the anthropogenic heat increases, in the nighttime, the relative importance of the UHI effect on local winds increases while the relative importance of the surface roughness effect on local winds decreases.

Fig. 13 shows the same fields presented in Fig. 12 except for the US1.7 and US2.2 simulations. In the daytime, the UHI and converging wind differences are stronger in the US1.7 and US2.2 simulations than in the URBAN simulation (Figs. 7c and 13a and b). In comparison with the URBAN simulation, the daytime-averaged UHI intensity in the urban areas increases by 0.19°C in the US1.7 simulation and by 0.30°C in the US2.2 simulation. The magnitudes of the wind difference averaged over the urban areas increase by 0.16 and 0.23 m s^{-1} in the US1.7 and US2.2 simulations, respectively. It is noted that the UHI southeast of Dhaka is considerably intensified with increasing urban size. In this region, the non-urban land cover is largely replaced with the urban land cover by increasing the urban size. Furthermore, a large portion of the non-urban area inside Dhaka is changed into the urban area. The warm urban air advected from Dhaka also contributes to the enhancement of the UHI southeast of Dhaka. Overall, in the daytime, the UHI and the UHI effect on local winds strengthen as the urban size increases.

Similar to the daytime, in the nighttime (Figs. 7f and 13c and d), the UHI overall strengthens with increasing urban size. Compared to the URBAN simulation, the nighttime-averaged UHI intensities in the urban areas increase by 0.58 and 0.86°C in the US1.7 and US2.2 simulations, respectively. The location of the maximum nighttime-averaged UHI intensity in the US1.7 and US2.2 simulations is found east of Dhaka, being further downwind compared to that in the URBAN simulation. As the urban size increases, the easterly-northeasterly wind differences are found over wider areas west and south of Dhaka. The magnitude of the wind difference averaged over the western region of Dhaka in both the US1.7 and US2.2 simulations slightly increases by 0.02 m s^{-1} , compared to that in the URBAN simulation. This indicates that the region where the surface roughness effect on local winds is important expands. Meanwhile, the converging wind differences downwind of Dhaka are enhanced with increasing urban size, being located in similar regions in the URBAN, US1.7, and US2.2 simulations. Compared to the URBAN simulation, the magnitudes of the wind difference averaged over the eastern region and near-downwind of Dhaka increase by 0.13 and 0.22 m s^{-1} in the US1.7 and US2.2 simulations,

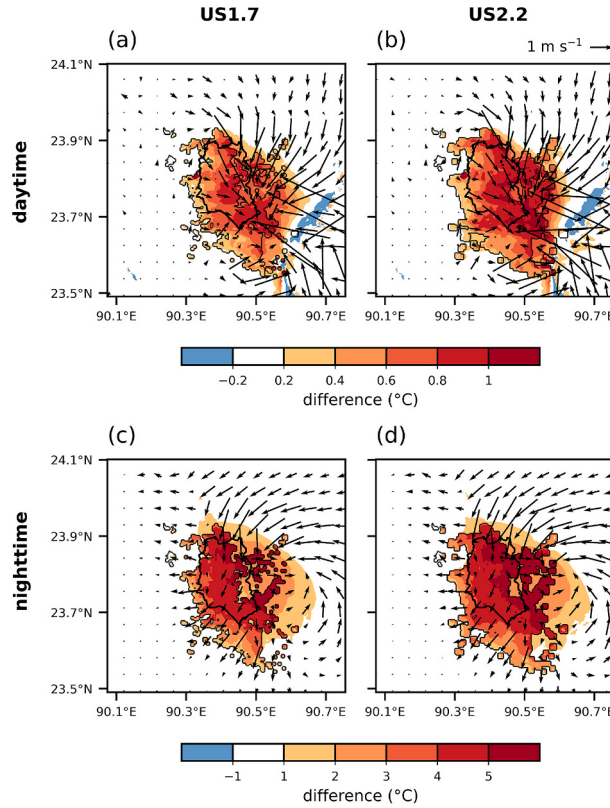


Fig. 13. Same as Fig. 12 except for the US1.7 (first column) and US2.2 (second column) simulations. The boundary of the urban areas in each simulation is indicated by the thin black solid line.

respectively. This indicates that as the urban size increases, the UHI effect on local winds downwind of Dhaka strengthens.

5. Summary and conclusions

Using the WRF model coupled with the SNUUCM, a single-layer urban canopy model, this study investigates urban effects on thermal and wind environments in the Dhaka metropolitan area. A case of hot days with weak synoptic forcing is selected for simulations, and detailed analyses of the differences between the urban and no-urban simulations are made. In the urban simulation, in the daytime, the sensible heat flux is considerably increased and the latent heat flux is greatly reduced. Convective activities in the daytime PBL are enhanced in the urban simulation. The UHI is much stronger in the nighttime than in the daytime. In the daytime, the UHI effect on local winds is found to be more important than the urban surface roughness effect on local winds although the UHI is much weaker in the daytime than in the nighttime. In the nighttime, interestingly, the relative importance of the UHI and urban surface roughness effects on local winds is found to differ depending on the region for given prevailing winds. Impacts of increases in anthropogenic heat and urban size on the UHI and the urban effects on local winds are examined. With increasing anthropogenic heat, in both daytime and nighttime, the UHI strengthens and the UHI effect on local winds is enhanced. With increasing urban size, in both daytime and nighttime, the UHI is intensified and the UHI effect on local winds is enhanced as well. The surface roughness effect appears in wider areas in the nighttime as the urban size increases.

Dhaka is a deltaic megacity with high population density, has experienced rapid urbanization, and is vulnerable to heat extremes. In this study, we quantitatively show how the presence of the urban areas in the Dhaka metropolitan area affects temperature and local winds during a hot day through high-resolution simulations. Particularly, this study reveals how the relative importance of the UHI effect and the surface roughness effect on local winds differs depending on the time of day and the region for given prevailing winds in the Dhaka metropolitan area, which was not explored in previous studies. Therefore, this study provides some insights into the urban thermal and mechanical effects on wind environments. However, this study only considers a single case with the Dhaka metropolitan area being under the influence of the synoptic high-pressure system. Since different synoptic weather can differently impact the UHI and the urban effects on local winds, how these UHI and urban effects appear under various synoptic weather conditions needs to be investigated for further understanding. Furthermore, a single combination of initial/boundary conditions and physics parameterization schemes is used for simulations in this study. Further investigations using various combinations of initial/boundary conditions and/or physics parameterization schemes will be helpful for more robust examinations of urban effects on thermal and wind environments.

The case days in this study are under heat waves. It is well known that UHIs can synergistically interact with heat waves (Li and Bou-Zeid, 2013; Park et al., 2023; Tabassum et al., 2024). It would be interesting to examine the interactions of the UHI with heat waves and the impacts of the interactions on local winds. Considering the severeness of air pollution in Dhaka (Rana et al., 2016; Pavel et al., 2021), it would be also interesting to examine how air quality is affected by the UHI and the urban effects on local winds. To better understand and cope with the weather- and climate-related risks Dhaka faces, extensive numerical simulation and observational studies of urban weather and climate in the Dhaka metropolitan area are required.

CRediT authorship contribution statement

Abeda Tabassum: Writing – review & editing, Writing – original draft, Visualization, Validation, Methodology, Investigation, Formal analysis, Data curation. **Seong-Ho Hong:** Writing – review & editing, Writing – original draft, Methodology, Formal analysis. **Kyeongjoo Park:** Writing – review & editing, Writing – original draft, Formal analysis. **Jong-Jin Baik:** Writing – review & editing, Writing – original draft, Supervision, Methodology, Formal analysis, Conceptualization.

Declaration of competing interest

The authors declare that they have no known competing financial interests or personal relationships that could have appeared to influence the work reported in this paper.

Data availability

Data will be made available on request.

Acknowledgements

We are grateful to one anonymous reviewer who provided valuable comment on this work. This work was supported by the National Research Foundation of Korea (NRF) under grant 2021R1A2C1007044.

References

- Abrahm, R., Sarkar, S.K., Nishtha, K.T., Talukdar, S., Shahfahad, Rahman, A., Islam, A.R.M.T., Mosavi, A., 2022. Assessing the spatial mapping of heat vulnerability under urban heat island (UHI) effect in the Dhaka Metropolitan Area. *Sustainability* 14, 4945.
- Ahmed, B., Kamruzzaman, M., Zhu, X., Rahman, M.S., Choi, K., 2013. Simulating land cover changes and their impacts on land surface temperature in Dhaka, Bangladesh. *Remote Sens.* 5, 5969–5998.
- Baik, J.-J., Lim, H., Han, B.-S., Jin, H.-G., 2022. Cool-roof effects on thermal and wind environments during heat waves: a case modeling study in Seoul, South Korea. *Urban Clim.* 41, 101044.
- Banghoff, J.R., Sorber, J.D., Stensrud, D.J., Young, G.S., Kumjian, M.R., 2020. A 10-year warm-season climatology of horizontal convective rolls and cellular convection in central Oklahoma. *Mon. Weather Rev.* 148, 21–42.
- BBS, 2022. Population and Housing Census 2022: Preliminary Report. Bangladesh Bureau of Statistics, Dhaka, 55 pp.
- Beck, H.E., Zimmermann, N.E., McVicar, T.R., Vergopolan, N., Berg, A., Wood, E.F., 2018. Present and future Köppen-Geiger climate classification maps at 1-km resolution. *Sci. Data* 5, 180214.
- Brandi, A., Martilli, A., Salamanca, F., Georgescu, M., 2024. Urban boundary-layer flows in complex terrain: dynamic interactions during a hot and dry summer season in Phoenix, Arizona. *Q. J. R. Meteorol. Soc.* 150, 3099–3116.
- Byomkesh, T., Nakagoshi, N., Dewan, A.M., 2012. Urbanization and green space dynamics in Greater Dhaka, Bangladesh. *Landsc. Ecol. Eng.* 8, 45–58.
- Choi, N., Lee, M.-I., 2019. Spatial variability and long-term trend in the occurrence frequency of heatwave and tropical night in Korea. *Asia-Pac. J. Atmos. Sci.* 55, 101–114.
- Chow, W.T.L., Roth, M., 2006. Temporal dynamics of the urban heat island of Singapore. *Int. J. Climatol.* 26, 2243–2260.
- Cotton, W.R., Pielke, R.A., 2007. Human Impacts on Weather and Climate. Cambridge University Press, 330 pp.
- Coutts, A.M., Beringer, J., Tapper, N.J., 2007. Impact of increasing urban density on local climate: spatial and temporal variations in the surface energy balance in Melbourne, Australia. *J. Appl. Meteorol. Climatol.* 46, 477–493.
- Danielson, J.J., Gesch, D.B., 2011. Global Multi-Resolution Terrain Elevation Data 2010 (GMTED2010). U.S. Geological Survey Open-File Report 2011–1073, Reston, VA, 26 pp.
- Das, M.K., Karmakar, S., 2015. Urban heat island assessment for a tropical urban air-shed in Bangladesh. In: ICUC9 - 9th International Conference on Urban Climate Jointly with 12th Symposium on the Urban Environment, Toulouse, France, pp. 20–24.
- Deng, J.-S., Wang, K., Li, J., Deng, Y.-H., 2009. Urban land use change detection using multisensor satellite images. *Pedosphere* 19, 96–103.
- Du, H., Zhan, W., Liu, Z., Li, J., Li, L., Lai, J., Miao, S., Huang, F., Wang, C., Wang, C., Fu, H., Jiang, L., Hong, F., Jiang, S., 2021. Simultaneous investigation of surface and canopy urban heat islands over global cities. *ISPRS J. Photogramm. Remote Sens.* 181, 67–83.
- Dudhia, J., 1989. Numerical study of convection observed during the Winter Monsoon Experiment using a mesoscale two-dimensional model. *J. Atmos. Sci.* 46, 3077–3107.
- Fernández, M.E., Picone, N., Gentili, J.O., Campo, A.M., 2021. Analysis of the Urban Energy Balance in Bahía Blanca (Argentina). *Urban Clim.* 37, 100856.
- Hersbach, H., Bell, B., Berrisford, P., Hirahara, S., Horányi, A., Muñoz-Sabater, J., Nicolas, J., Peubey, C., Radu, R., Schepers, D., Simmons, A., Soci, C., Abdalla, S., Abellán, X., Balsamo, G., Bechtold, P., Biavati, G., Bidlot, J., Bonavita, M., De Chiara, G., Dahlgren, P., Dee, D., Diamantakis, M., Dragani, R., Flemming, J., Forbes, R., Fuentes, M., Geer, A., Haimes, L., Healy, S., Hogan, R.J., Hölm, E., Janisková, M., Keeley, S., Laloyaux, P., Lopez, P., Lupu, C., Radnoti, G., de Rosnay, P., Rozum, I., Vamborg, F., Villaume, S., Thépaut, J.-N., 2020. The ERA5 global reanalysis. *Q. J. R. Meteorol. Soc.* 146, 1999–2049.
- Hong, S.-Y., Noh, Y., Dudhia, J., 2006. A new vertical diffusion package with an explicit treatment of entrainment processes. *Mon. Weather Rev.* 134, 2318–2341.
- Hong, S.-H., Jin, H.-G., Baik, J.-J., 2024. Impacts of background wind on the interactions between urban breeze circulation and convective cells: ensemble large-eddy simulations. *Q. J. R. Meteorol. Soc.* 150, 1518–1537.
- Imran, H.M., Hossain, A., Islam, A.K.M.S., Rahman, A., Bhuiyan, M.A.E., Paul, S., Alam, A., 2021. Impact of land cover changes on land surface temperature and human thermal comfort in Dhaka city of Bangladesh. *Earth Syst. Environ.* 5, 667–693.

- Jiménez, P.A., Dudhia, J., González-Rouco, J.F., Navarro, J., Montávez, J.P., García-Bustamante, E., 2012. A revised scheme for the WRF surface layer formulation. *Mon. Weather Rev.* 140, 898–918.
- Kain, J.S., 2004. The Kain-Fritsch convective parameterization: an update. *J. Appl. Meteorol.* 43, 170–181.
- Kang, H.-Q., Zhu, B., Zhu, T., Sun, J.-L., Ou, J.-J., 2014. Impact of megacity Shanghai on the urban heat-island effects over the downstream city Kunshan. *Bound.-Layer Meteorol.* 152, 411–426.
- Knievel, J.C., Bryan, G.H., Hacker, J.P., 2007. Explicit numerical diffusion in the WRF model. *Mon. Weather Rev.* 135, 3808–3824.
- Kotharkar, R., Ghosh, A., 2021. Review of heat wave studies and related urban policies in South Asia. *Urban Clim.* 36, 100777.
- Kuang, W., Dou, Y., Zhang, C., Chi, W., Liu, A., Liu, Y., Zhang, R., Liu, J., 2015. Quantifying the heat flux regulation of metropolitan land use/land cover components by coupling remote sensing modeling with in situ measurement. *J. Geophys. Res. Atmos.* 120, 113–130.
- Lee, S.-H., Baik, J.-J., 2010. Statistical and dynamical characteristics of the urban heat island intensity in Seoul. *Theor. Appl. Climatol.* 100, 227–237.
- LeMone, M.A., 1973. The structure and dynamics of horizontal roll vortices in the planetary boundary layer. *J. Atmos. Sci.* 30, 1077–1091.
- Lemonsu, A., Masson, V., 2002. Simulation of a summer urban breeze over Paris. *Bound.-Layer Meteorol.* 104, 463–490.
- Li, D., Bou-Zeid, E., 2013. Synergistic interactions between urban heat islands and heat waves: the impact in cities is larger than the sum of its parts. *J. Appl. Meteorol. Climatol.* 52, 2051–2064.
- Lim, K.-S.S., Hong, S.-Y., 2010. Development of an effective double-moment cloud microphysics scheme with prognostic cloud condensation nuclei (CCN) for weather and climate models. *Mon. Weather Rev.* 138, 1587–1612.
- Mannan, M.A., Akter, F., Rashid, M.B., Hossain, M.M., Faruque, S.O., Ara, S.S., Sultana, A., Barua, S., Karmakar, S., Chowdhury, M.A.M., 2022. An analytical study of Heat Wave occurred over Bangladesh during pre-monsoon of 2021. *Dew-drop* 8, 152–160.
- Memon, R.A., Leung, D.Y.C., Liu, C., 2008. A review on the generation, determination and mitigation of Urban Heat Island. *J. Environ. Sci.* 20, 120–128.
- Mlawer, E.J., Taubman, S.J., Brown, P.D., Iacono, M.J., Clough, S.A., 1997. Radiative transfer for inhomogeneous atmospheres: RRTM, a validated correlated-k model for the longwave. *J. Geophys. Res. Atmos.* 102, 16663–16682.
- Montes, C., Acharya, N., Hassan, S.M.Q., Krupnik, T., 2021. Intense precipitation events during the monsoon season in Bangladesh as captured by satellite-based products. *J. Hydrometeorol.* 22, 1405–1419.
- Nissan, H., Burkart, K., de Perez, E.C., Van Aalst, M., Mason, S., 2017. Defining and predicting heat waves in Bangladesh. *J. Appl. Meteorol. Climatol.* 56, 2653–2670.
- Oke, T.R., Fugle, R.F., 1972. Comparison of urban/rural counter and net radiation at night. *Bound.-Layer Meteorol.* 2, 290–308.
- Park, K., Jin, H.-G., Baik, J.-J., 2023. Contrasting interactions between urban heat islands and heat waves in Seoul, South Korea, and their associations with synoptic patterns. *Urban Clim.* 49, 101524.
- Pavel, M.R.S., Zaman, S.U., Jeba, F., Islam, M.S., Salam, A., 2021. Long-term (2003–2019) air quality, climate variables, and human health consequences in Dhaka, Bangladesh. *Front. Sustain. Cities* 3, 681759.
- Phelan, P.E., Kaloush, K., Miner, M., Golden, J., Phelan, B., Silva III, H., Taylor, R.A., 2015. Urban heat island: mechanisms, implications, and possible remedies. *Annu. Rev. Environ. Resour.* 40, 285–307.
- Rajeswari, J.R., Srinivas, C.V., Venkatraman, B., 2022. Impact of urbanization on boundary-layer parameters and mesoscale circulations over tropical coastal city, Chennai. *Meteorol. Atmos. Phys.* 134, 3.
- Ramamurthy, P., Bou-Zeid, E., Smith, J.A., Wang, Z., Baeck, M.L., Saliendra, N.Z., Hom, J.L., Welty, C., 2014. Influence of subfacet heterogeneity and material properties on the urban surface energy budget. *J. Appl. Meteorol. Climatol.* 53, 2114–2129.
- Rana, M.M., Sulaiman, N., Sivertsen, B., Khan, M.F., Nasreen, S., 2016. Trends in atmospheric particulate matter in Dhaka, Bangladesh, and the vicinity. *Environ. Sci. Pollut. Res.* 23, 17393–17403.
- Raziq, A., Xu, A., Li, Y., Zhao, Q., 2016. Monitoring of land use/land cover changes and urban sprawl in Peshawar city in Khyber Pakhtunkhwa: an application of geo-information techniques using of multi-temporal satellite data. *J. Remote Sens. GIS* 5, 1000174.
- Roy, D.P., Wulder, M.A., Loveland, T.R., Woodcock, C.E., Allen, R.G., Anderson, M.C., Helder, D., Irons, J.R., Johnson, D.M., Kennedy, R., Scambos, T.A., Schaaf, C.B., Schott, J.R., Sheng, Y., Vermote, E.F., Belward, A.S., Bindschadler, R., Cohen, W.B., Gao, F., Hippel, J.D., Hostert, P., Huntington, J., Justice, C.O., Kilic, A., Kovalskyy, V., Lee, Z.P., Lymburner, L., Masek, J.G., McCorkel, J., Shuai, Y., Trezza, R., Vogelmann, J., Wynne, R.H., Zhu, Z., 2014. Landsat-8: science and product vision for terrestrial global change research. *Remote Sens. Environ.* 145, 154–172.
- Ryu, Y.-H., Baik, J.-J., 2013. Daytime local circulations and their interactions in the Seoul metropolitan area. *J. Appl. Meteorol. Climatol.* 52, 784–801.
- Ryu, Y.-H., Baik, J.-J., Lee, S.-H., 2011. A new single-layer urban canopy model for use in mesoscale atmospheric models. *J. Appl. Meteorol. Climatol.* 50, 1773–1794.
- Ryu, Y.-H., Baik, J.-J., Han, J.-Y., 2013a. Daytime urban breeze circulation and its interaction with convective cells. *Q. J. R. Meteorol. Soc.* 139, 401–413.
- Ryu, Y.-H., Baik, J.-J., Lee, S.-H., 2013b. Effects of anthropogenic heat on ozone air quality in a megacity. *Atmos. Environ.* 80, 20–30.
- Sismanidis, P., Keramitsoglou, I., Kiranoudis, C.T., 2015. Diurnal analysis of surface Urban Heat Island using spatially enhanced satellite derived LST data. In: 2015 Joint Urban Remote Sensing Event (JURSE), Lausanne, Switzerland, pp. 1–4.
- Skamarock, W.C., Klemp, J.B., Dudhia, J., Gill, D.O., Liu, Z., Berner, J., Wang, W., Powers, J.G., Duda, M.G., Barker, D.M., Huang, X.-Y., 2019. A Description of the Advanced Research WRF Model Version 4. NCAR Tech. Note TN-556+STR.
- Sugawara, H., Takamura, T., 2014. Surface albedo in cities: case study in Sapporo and Tokyo, Japan. *Bound.-Layer Meteorol.* 153, 539–553.
- Sulla-Menashe, D., Friedl, M.A., 2018. User Guide to Collection 6 MODIS Land Cover (MCD12Q1 and MCD12C1) Product. USGS, Reston, VA, 18 pp.
- Tabassum, A., Park, K., Seo, J.-M., Han, J.-Y., Baik, J.-J., 2024. Characteristics of the urban heat island in Dhaka, Bangladesh, and its interaction with heat waves. *Asia-Pac. J. Atmos. Sci.* 60, 479–493.
- Tan, J., Zheng, Y., Tang, X., Guo, C., Li, L., Song, G., Zhen, X., Yuan, D., Kalkstein, A.J., Li, F., Chen, H., 2010. The urban heat island and its impact on heat waves and human health in Shanghai. *Int. J. Biometeorol.* 54, 75–84.
- Tewari, M., Chen, F., Wang, W., Dudhia, J., LeMone, M.A., Mitchell, K., Ek, M., Gayno, G., Wegiel, J., Cuenca, R.H., 2004. Implementation and verification of the unified Noah land surface model in the WRF model. In: 20th Conference on Weather Analysis and Forecasting/16th Conference on Numerical Weather Prediction, Seattle, WA, USA, pp. 10–15.
- Uddin, A.S.M.S., Khan, N., Islam, A.R.M.T., Kamruzzaman, M., Shahid, S., 2022. Changes in urbanization and urban heat island effect in Dhaka city. *Theor. Appl. Climatol.* 147, 891–907.
- UN DESA, 2019. World Urbanization Prospects 2018: Highlights. United Nations, Department of Economic and Social Affairs, New York, 555 pp.
- Wacker, A.G., Landgrebe, D.A., 1972. Minimum distance classification in remote sensing. In: LARS Technical Reports., 25 pp.
- Wang, X., Li, Y., 2016. Predicting urban heat island circulation using CFD. *Build. Environ.* 99, 82–97.
- Wang, L., Li, D., 2021. Urban heat islands during heat waves: a comparative study between Boston and Phoenix. *J. Appl. Meteorol. Climatol.* 60, 621–641.
- Wang, Q., Hang, J., Fan, Y., Li, Y., 2020a. Urban plume characteristics under various wind speed, heat flux, and stratification conditions. *Atmos. Environ.* 239, 117774.
- Wang, Q., Zhang, C., Ren, C., Hang, J., Li, Y., 2020b. Urban heat island circulations over the Beijing-Tianjin region under calm and fair conditions. *Build. Environ.* 180, 107063.
- Weng, Q., 2012. Remote sensing of impervious surfaces in the urban areas: requirements, methods, and trends. *Remote Sens. Environ.* 117, 34–49.
- Wever, N., 2012. Quantifying trends in surface roughness and the effect on surface wind speed observations. *J. Geophys. Res. Atmos.* 117, D11104.
- Wouters, H., De Ridder, K., Demuzere, M., Lauwaet, D., van Lipzig, N.P.M., 2013. The diurnal evolution of the urban heat island of Paris: a model-based case study during Summer 2006. *Atmos. Chem. Phys.* 13, 8525–8541.
- Wu, Y., Zhao, K., Huang, J., Arend, M., Gross, B., Moshary, F., 2019. Observation of heat wave effects on the urban air quality and PBL in New York City area. *Atmos. Environ.* 218, 117024.
- Xue, J., Zong, L., Yang, Y., Bi, X., Zhang, Y., Zhao, M., 2023. Diurnal and interannual variations of canopy urban heat island (CUHI) effects over a mountain–valley city with a semi-arid climate. *Urban Clim.* 48, 101425.
- Yang, P., Ren, G., Yan, P., Deng, J., 2020. Tempospatial pattern of surface wind speed and the “Urban Stilling Island” in Beijing City. *J. Meteorol. Res.* 34, 986–996.

- Yi, C., Kwon, H.-G., Yang, H., 2022. Spatial temperature differences in local climate zones of Seoul metropolitan area during a heatwave. *Urban Clim.* 41, 101012.
- Zhang, N., Wang, X., Peng, Z., 2014. Large-eddy simulation of mesoscale circulations forced by inhomogeneous urban heat island. *Bound.-Layer Meteorol.* 151, 179–194.
- Zhang, D.-L., Jin, M.S., Shou, Y., Dong, C., 2019. The influences of urban building complexes on the ambient flows over the Washington–Reston region. *J. Appl. Meteorol. Climatol.* 58, 1325–1336.
- Zheng, Z., Lin, X., Chen, L., Yan, C., Sun, T., 2024. Effects of urbanization and topography on thermal comfort during a heat wave event: a case study of Fuzhou, China. *Sust. Cities Soc.* 102, 105233.
- Zhou, J., Chen, Y., Zhang, X., Zhan, W., 2013. Modelling the diurnal variations of urban heat islands with multi-source satellite data. *Int. J. Remote Sens.* 34, 7568–7588.